Angle-resolved photoelectron study on the structures of silicon nitride films and Si3N4/Si interfaces formed using nitrogen-hydrogen radicals

doi: 10.1063/1.3002418

Angle-resolved photoelectron study on the structures of silicon nitride films and Si_3N_4/Si interfaces formed using nitrogen-hydrogen radicals

Takashi Aratani,[1] Masaaki Higuchi,[1,a)] Shigetoshi Sugawa,[1] Eiji Ikenaga,[2] Jiro Ushio,[3] Hiroshi Nohira,[4] Tomoyuki Suwa,[5,b)] Akinobu Teramoto,[5] Tadahiro Ohmi,[5] and Takeo Hattori[5]

[1]*Graduate School of Engineering, Tohoku University, Aza-Aoba, Aramaki, Aoba-ku, Sendai 980-8579, Japan*
[2]*JASRI/Spring-8, Kouto, Mikazuki, Hyogo 679-5198, Japan*
[3]*Advanced Research Laboratory, Hitachi Ltd., Hitachi-shi, Ibaraki 319-1292, Japan*
[4]*Musashi Institute of Technology, Tamazutsumi, Setagaya-ku, Tokyo 158-8857, Japan*
[5]*New Industry Creation Hatchery Center, Tohoku University, Aza-Aoba, Aramaki, Aoba, Sendai 980-8579, Japan*

(Received 22 July 2008; accepted 7 September 2008; published online 11 December 2008)

Soft x-ray-excited angle-resolved photoemission results for nitride films formed using nitrogen–hydrogen radicals on Si(100), Si(111), and Si(110) are reported. The data were obtained using synchrotron radiation, which allowed the Si 2*p*, N 1*s*, and O 1*s* levels to be investigated with the same probing depth. The following main results were obtained: (1) the Si_3N_4 film is covered with one monolayer of $Si-(OH)_3N$. Its areal density is 15% smaller on Si(111) than on Si(100) and Si(110), (2) the Si_3N_4/Si interfaces on all three surfaces are compositionally abrupt. This conclusion is based on the observation that no Si atoms bonded with three N atoms and one Si atom were detected, and (3) the observation that the number of Si–H bonds at the Si_3N_4/Si(110) interface is 38%–53% larger than those at the Si_3N_4/Si(100) and Si_3N_4/Si(111) interfaces indicates a dependence of the interface structure on the orientation of the substrate. © *2008 American Institute of Physics*. [DOI: 10.1063/1.3002418]

I. INTRODUCTION

High-κ gate dielectrics with a low leakage current are highly anticipated for advanced ultralarge-scale integrations (ULSIs).[1] Si_3N_4 film formed using nitrogen–hydrogen (NH) radicals is attractive as a high-κ gate dielectric owing to its high relative dielectric constant (7.5), sufficiently low interface state density for application in metal-oxide-semiconductor devices,[2,3] and as a Si-based dielectric. In 1978 Ito *et al.*[4] succeeded in growing uniform nitride films with thicknesses of less than 10 nm by the thermal reaction of Si(100) with nitrogen gas. Hayafuji and Kajiwara[5] found that during the thermal nitridation of Si(100) in NH_3 nitride-film growth is almost independent of NH_3 pressure. Maillot *et al.*[6] proposed possible atomic transport mechanisms during the thermal nitridation of Si in NH_3 using ^{15}N. From the photoemission arising from the Si 2*p* and N 1*s* core levels in thin nitride films grown *in situ* by the high-temperature reaction of Si(100) with NH_3, Peden *et al.*[7] found that a Si monolayer exists as the outermost surface layer on top of a Si_3N_4 film.

In our previous study[8] we measured soft x-ray-excited angle-resolved photoemission from the Si 2*p*, N 1*s*, and O 1*s* core levels and the valence band with the same probing depth for silicon nitride films formed on Si(100), Si(111), and Si(110) using NH radicals. From the analyses of these spectra we found that nitride films were covered with thin silicon oxide films, and interface layers consisting of the intermediate nitridation states of Si (abbreviated hereafter as subnitrides) were formed between nitride film and Si substrate. In the nitride film formed on Si(100), N atoms were found to connect silicon oxide film and silicon nitride film. Furthermore, it was found that the crystal orientation of the Si substrate has no effect on the valence band offset at the Si_3N_4/Si interface.

In this study, the photoelectron spectra arising from subnitrides were successfully extracted from the angle-resolved photoelectron spectra and used to clarify the effect of the crystallographic orientation of the Si substrate on the Si_3N_4/Si interface structure. Furthermore, the abruptness of compositional transition at the Si_3N_4/Si interface and the structure of silicon nitride film were also clarified by angle-resolved photoelectron spectroscopy.

II. EXPERIMENTAL DETAILS

Because the Si_3N_4 film required for advanced ULSIs must be ultrathin, the characterization and control of the Si_3N_4/Si interface structure on the atomic scale are essential. In this study, we measured the angle-resolved photoemission from the Si 2*p* and N 1*s* core levels in nitride films with a high energy resolution and an appropriately large electron escape depth. Because the thicknesses of the nitride films are nearly 1 nm, the electron escape depth of nearly 2 nm and highly brilliant synchrotron radiation are necessary in detecting the angle-resolved photoemission from the Si_3N_4/Si interface through the Si_3N_4 film, and a high energy resolution

a)Present address: Toshiba Corporation, Semiconductor Company, 8 Shinsugita-cho, Isogo-ku, Yokohama, 235-8582, Japan.
b)Author to whom correspondence should be addressed. Electronic mail: suwa@fff.niche.tohoku.ac.jp.

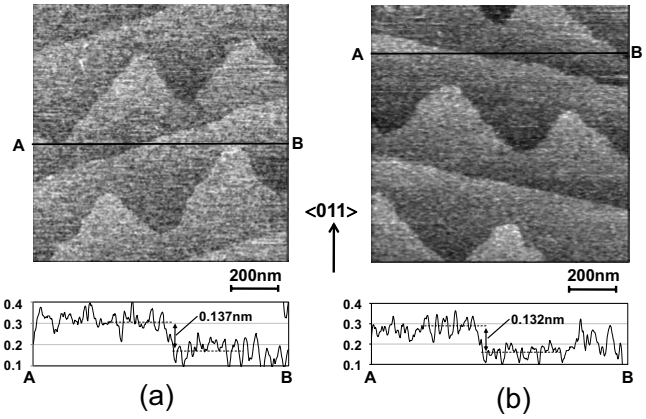

FIG. 1. AFM images and cross-sectional profiles along the lines from A to B shown in the AFM images. Steps, whose heights are almost equal to a single atomic step height of 0.135 nm on Si(100), are observed in AFM images (a) before the nitridation and (b) after 2.3-nm-thick nitride film was formed at 600 °C using NH radicals, which were produced in a microwave-excited high-density Xe/NH_3 mixture plasma at a pressure of 8 Pa.

of 100 meV is necessary to resolve the composition of subnitrides localized at the Si_3N_4/Si interface. Furthermore, to simply determine the compositional depth profile, the kinetic energies, which govern the electron escape depths,[9] of photoelectrons emitted from Si 2*p*, N 1*s*, and O 1*s* core levels were adjusted to be equal by choosing appropriate photon energies (PEs) for each core level. Such measurements could be performed at Super Photon Ring 8 GeV (SPring-8).

The wafers used in this study are *n*-type Si(100), Si(110), and Si(111) substrates whose resistivities are nearly 10 Ω cm. The atomically smooth substrates were prepared by the following processes. The wet oxidation of these substrates was performed at 1100 °C to form 1-μm-thick oxide films. After etching the oxide films in HCl/HF mixture solution,[10] the substrates were cleaned in five steps at room temperature.[11] After cleaning, the surface microroughness (Ra) of these cleaned substrates measured by atomic force microscopy (AFM) was 0.08 nm. Then, the nitridation of these cleaned substrates was performed at the same time at 600 °C using NH radicals, which were produced in a microwave-excited high-density Xe/NH_3 mixture plasma[12] at a pressure of 20 Pa, and the nitride films thus formed were kept in dry N_2 until their photoelectron spectra were measured. The microwave frequency and power were 2.45 GHz and 5 W/cm^2, respectively.

III. EXPERIMENTAL RESULTS AND DISCUSSION

A. Structure of the nitride films

Figure 1 shows the influence of nitridation on the surface morphology of Si(100) observed by AFM. According to this figure, steps, whose heights are almost equal to a single atomic step height of 0.135 nm on Si(100), observed before the nitridation are preserved after the nitridation. This implies that the nitridation proceeds uniformly on an atomic scale. Figures 2 and 3 show the N 1*s* and O 1*s* spectra arising from the nitride films thus formed on Si(100), Si(111), and Si(110) measured at a photoelectron takeoff angle (TOA) of 80° and PEs of 1349 and 1481 eV, respectively. The values

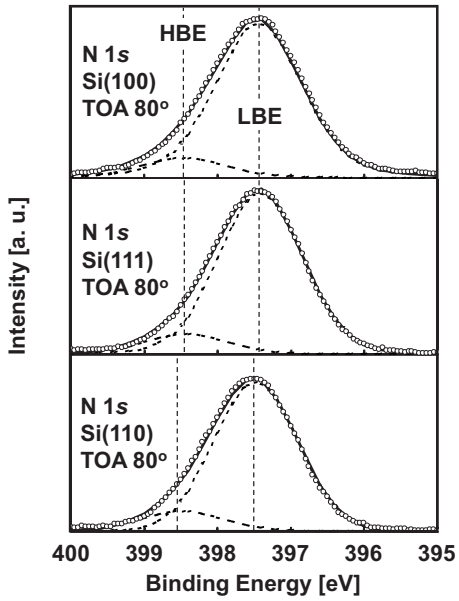

FIG. 2. N 1*s* spectra measured at TOA of 80° for nitride films formed on Si(100), Si(111), and Si(110). N 1*s* spectra can be decomposed to spectra having a LBE and those having a HBE.

of 397.33, 397.30, and 397.48 eV, which were observed for binding energies (BEs) of the N 1*s* spectrum peaks originating from the nitride films formed on Si(100), Si(111), and Si(110), respectively, indicate that most of the N atoms contribute to form Si_3N_4 films.[7] The values of 532.29, 532.20, and 532.20 eV, which were observed for BEs of the O 1*s* spectrum peaks originating from the nitride films formed on Si(100), Si(111), and Si(110), respectively, indicate that all O atoms contribute to form Si–OH bonds.[13] Si–OH bonds were formed by the oxidation of pure Si layer, which exists on the surface of a Si_3N_4 film after the nitridation of Si,[7] in air just after the nitride film was removed from the nitridation chamber. Figure 4 shows the intensity ratio I(O 1*s*)/I(N 1*s*) as a

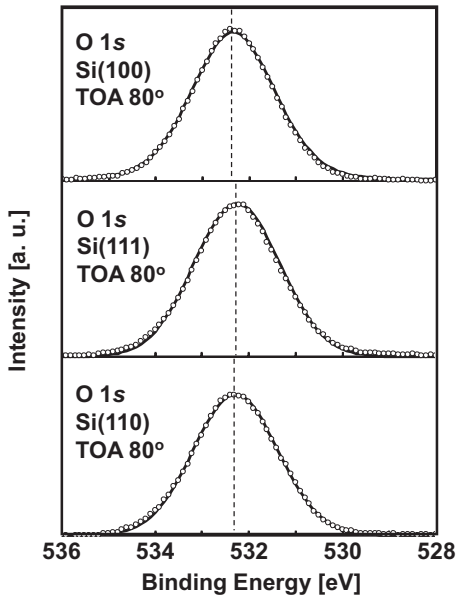

FIG. 3. O 1*s* spectra measured at TOA of 80° for nitride films formed on Si(100), Si(111), and Si(110).

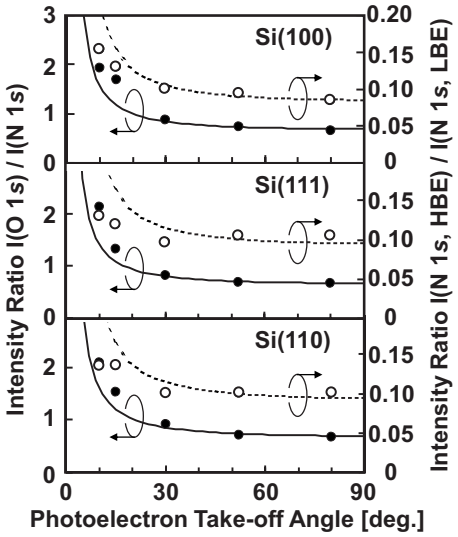

FIG. 4. Intensity ratios I(O 1*s*)/I(N 1*s*) and I(N 1*s*, HBE)/I(N 1*s*, LBE) as a function of TOA for nitride films formed on Si(100), Si(111), and Si(110). I(O 1*s*) and I(N 1*s*) denote the O 1*s* and N 1*s* spectral intensities, respectively. I(N 1*s*, LBE) and I(N 1*s*, HBE) denote the N 1*s* spectra having LBE and those having HBE, respectively. Solid and dashed lines were calculated using parameters listed in Table I.

function of TOA for the films formed on Si(100), Si(111), and Si(110). Here, I(O 1*s*) and I(N 1*s*) denote O 1*s* and N 1*s* spectral intensities, respectively.

As shown in Fig. 2, the N 1*s* spectra arising from the nitride films formed on Si(100), Si(111), and Si(110) can be decomposed into large peaks with a low BE (LBE) of 397.33, 397.30, and 397.48 eV, respectively, and small peaks with a high BE (HBE) of 398.33, 398.30, and 398.48 eV, respectively. Here, the full width at half maximum (FWHM) of large and small peaks is adjusted to be the same. According to a theoretical study of the BE of the N 1*s* core level,[14,15] a small peak can be correlated with a N atom that has three Si atoms as its first nearest neighbors and three N atoms and six O atoms as its second nearest neighbors, and hereafter referred to as an interface N atom because of the following reason. If the interface N atoms having areal densities expressed by D(N) listed in Table I localize at the $Si-N_4/Si-(OH)_3N$ interface as shown in Fig. 5, the dashed lines in Fig. 4 are obtained for the calculated dependence of the intensity ratio I(N 1*s*, HBE)/I(N 1*s*, LBE) on TOA. Here, I(N 1*s*, LBE) and I(N 1*s*, HBE), whose expressions are given in Appendix, denote the intensities of the large and small

TABLE I. Experimental values of the parameters required for a quantitative description of Si 2*p*, N 1*s*, and O 1*s* core-level intensities (see Sec. III).

	Si(100)	Si(111)	Si(110)
d_N	0.93 nm	0.78 nm	0.90 nm
D(Si–(OH)$_3$N)	6.5×10^{18} m^{-2}	5.7×10^{18} m^{-2}	6.8×10^{18} m^{-2}
D(N)	3.4×10^{18} m^{-2}	2.9×10^{18} m^{-2}	3.4×10^{18} m^{-2}
D(Si–Si$_3$H)	4.0×10^{18} m^{-2}	3.6×10^{18} m^{-2}	5.5×10^{18} m^{-2}
D[Si^{1+}(N)]	1.2×10^{18} m^{-2}	1.1×10^{18} m^{-2}	1.3×10^{18} m^{-2}
D(Si–Si$_2$NH)	1.9×10^{18} m^{-2}	1.6×10^{18} m^{-2}	2.1×10^{18} m^{-2}
D[Si^{2+}(N)]	0.5×10^{18} m^{-2}	0.4×10^{18} m^{-2}	0.6×10^{18} m^{-2}
D(I)	7.6×10^{18} m^{-2}	6.7×10^{18} m^{-2}	9.5×10^{18} m^{-2}

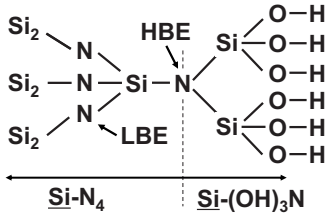

FIG. 5. Bonding configuration near Si–$(OH)_3N$/Si–N_4 interface which produces the N 1*s* spectra having LBE and those having HBE in Fig. 2.

peaks in Fig. 2, respectively. The parameters used in the calculation of the dashed lines are listed in Table I. Therefore, the silicon oxide film having bonding configuration of Si–$(OH)_3N$ is connected to the Si_3N_4 film by the interface N atoms as shown in Fig. 5.

From these findings, we can conclude that the structures of the nitride films formed on Si(100), Si(111), and Si(110) are almost the same. Here, as shown in Fig. 5 that N atoms, which produce LBE of N 1*s* spectra, contribute to form Si_3N_4.

B. Structure of compositional transition layers at Si_3N_4/Si interface

Figure 6 shows the Si $2p_{3/2}$ spectra arising from the nitride films formed on Si(100), Si(111), and Si(110) measured at a TOA of 80° and a PE of 1050 eV. After removing the background signal based on Tougaard's method from the observed spectrum,[16] the spectrum is decomposed into the Si $2p_{1/2}$ and Si $2p_{3/2}$ spin-orbit partner lines. In this decomposition, it was assumed that the spin-orbit splitting of the Si 2*p* spectra is 0.608 eV and the Si $2p_{1/2}$ to Si $2p_{3/2}$ intensity ratio is 0.5.[17] Other analytical details were described elsewhere.[16] In this figure Si $2p_{3/2}$ spectra arising from Si–$(OH)_3N$, Si–N_4, which contributes to form Si_3N_4, and bulk Si are decomposed. From the dependence of these decomposed spectral intensities on TOA, the intensity ratio

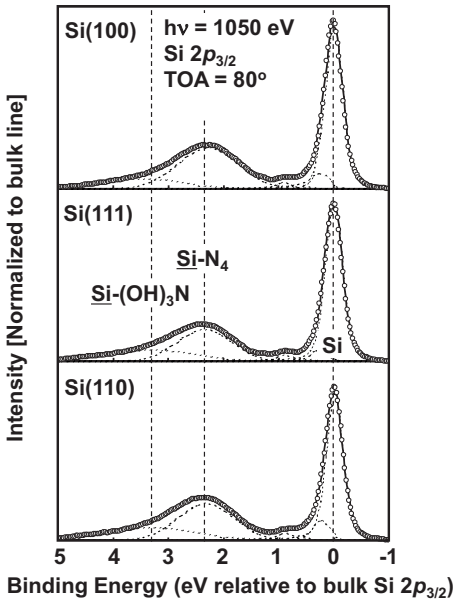

FIG. 6. Si $2p_{3/2}$ spectra measured at TOA of 80° for the nitride films formed on Si(100), Si(111), and Si(110).

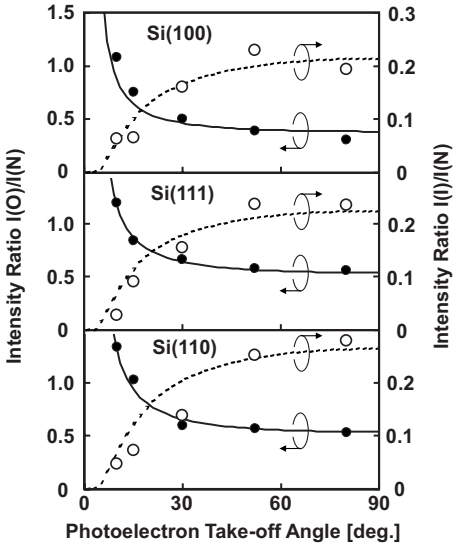

FIG. 7. Intensity ratios I(O)/I(N) and I(I)/I(N) as functions of TOA for nitride films formed on Si(100), Si(111), and Si(110). I(O), I(N), and I(I) denote intensities of the Si $2p_{3/2}$ spectrum arising from $\underline{Si}-(OH)_3N$, $\underline{Si}-N_4$, and all subnitrides, respectively. Solid and dashed lines were calculated using parameters listed in Table I.

I(O)/I(N) as a function of TOA shown in Fig. 7 and the intensity ratio I(N)/I(S) as a function of TOA shown in Fig. 8 were obtained. Here, I(O), I(N), and I(S), whose expressions are given in Appendix, denote the intensity of the Si $2p_{3/2}$ spectrum arising from $\underline{Si}-(OH)_3N$, $\underline{Si}-N_4$, and bulk Si, respectively.

If we assume that Si_3N_4 film having thickness expressed by d_N listed in Table I is covered with one monolayer of $\underline{Si}-(OH)_3N$ having areal density expressed by $D(\underline{Si}-(OH)_3N)$ listed in Table I, the solid lines in Figs. 4, 7, and 8 were obtained for the calculated dependence of the intensity ratios I(O 1*s*)/I(N 1*s*), I(O)/I(N), and I(N)/I(S) on

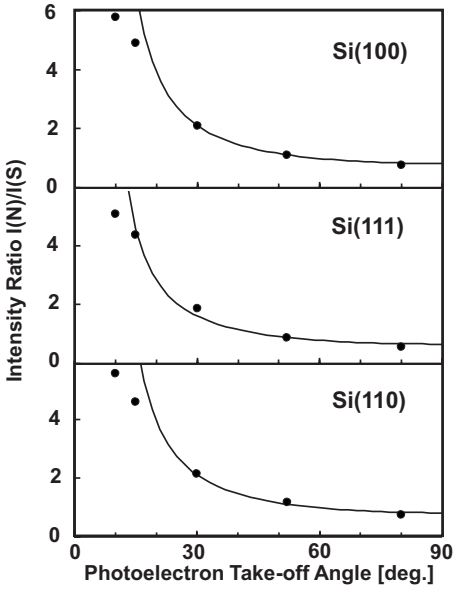

FIG. 8. Intensity ratio I(N)/I(S) as a function of TOA for nitride films formed on Si(100), Si(111), and Si(110). I(S) denotes intensity of the Si $2p_{3/2}$ spectrum arising from bulk Si. Solid lines were calculated using parameters listed in Table I.

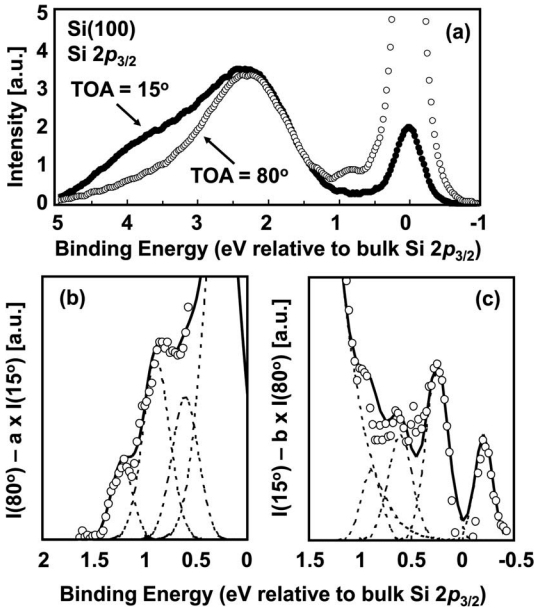

FIG. 9. (a) Si $2p_{3/2}$ spectrum measured at TOAs of 15° and 80° for nitride film formed on Si(100), (b) spectrum obtained by taking difference between two spectra in (a) to eliminate spectra arising from the nitride film, and (c) spectrum obtained by taking difference between two spectra in (a) to eliminate spectra arising from bulk Si.

TOA, respectively. Here, the expressions of I(O 1*s*) and I(N 1*s*) are given in Appendix and a value of (h/g) in the expression of I(O 1*s*)/I(N 1*s*) is adjusted so as to obtain the least-squares fit of calculated values of I(O 1*s*)/I(N 1*s*) to the experimental data. The parameters used in the calculation of these solid lines are listed in Table I. Here, the parameters used in the calculation of I(N)/I(S) are adjusted so as to obtain the least-squares fit of the solid lines in Fig. 8 with the experimental data for large TOA, where the effects of photoelectron diffraction on I(S) are small.[18] Deviations of the experimental data from the solid lines observed for small TOA in Fig. 8 must be attributed to photoelectron diffraction.[18] The values of $D(\underline{Si}-(OH)_3N)$ were determined from the analyses of I(O)/I(N) and I(N)/I(S). The excellent agreement of 2D(N) with $D(\underline{Si}-(OH)_3N)$ and the observation of O 1*s* spectra arising from Si–OH bonds requires the formation of $\underline{Si}-(OH)_3N$ on the surface of Si_3N_4 film as shown in Fig. 5. According to Table I, the thickness of the Si_3N_4 film formed on Si(111) is slightly smaller than those formed on Si(100) and Si(110) if we assume the same areal density of Si_3N_4. However, if we assume that the areal density of Si_3N_4 formed on Si(111) is 15% smaller than those of Si_3N_4 formed on Si(100) and Si(110) as in the case of D(N), the thickness of Si_3N_4 layer formed on Si(111) increases up to 0.91 nm, which is comparable to the thicknesses of Si_3N_4 layers formed on Si(100) and Si(110).

Figure 9(a) shows the Si $2p_{3/2}$ spectra arising from the nitride films formed on Si(100) measured at TOAs of 80° and 15° and a PE of 1050 eV. The spectrum arising from Si_3N_4/Si(100) interface shown in Fig. 9(b), in which the spectra having chemical shifts (CSs) of 0.89 and 1.23 eV are resolved, was obtained by subtracting the spectrum measured at a TOA of 15° from the spectrum measured at 80°, to eliminate spectrum arising from the nitride film after multi-

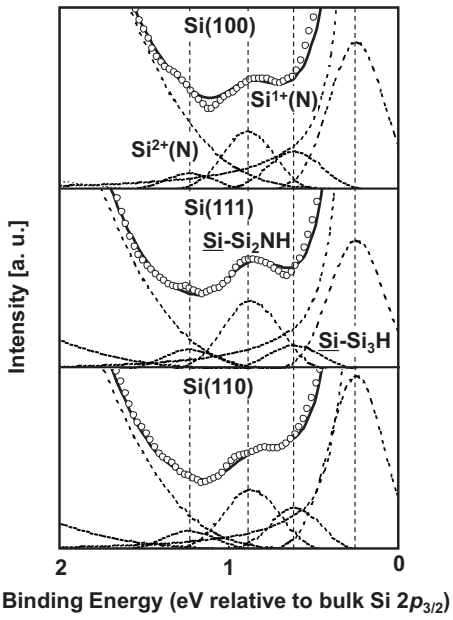

FIG. 10. Si $2p_{3/2}$ spectra measured at TOA of 80° for the nitride films formed on Si(100), Si(111), and Si(110). Subnitride spectra are decomposed using the BEs of Si $2p_{3/2}$ spectra arising from the components of subnitrides determined for Si(100).

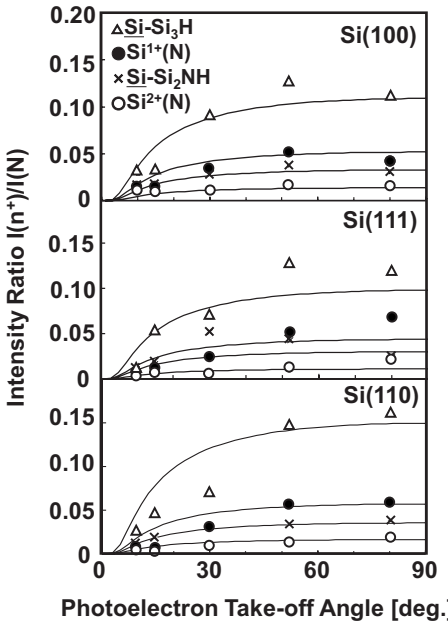

FIG. 11. Intensity ratio $I(n^+)/I(N)$ as a function of TOA for nitride films formed on Si(100), Si(111), and Si(110). $I(n^+)$ denotes the Si $2p_{3/2}$ spectral intensity arising from component of subnitrides. Solid lines were calculated using parameters listed in Table I.

plying the spectrum measured at a TOA of 15° by an appropriate factor of a. The spectrum arising from $Si_3N_4/Si(100)$ interface shown in Fig. 9(c), in which the spectra having CSs of 0.25, 0.61, and −0.20 eV are resolved, was obtained by subtracting the spectrum measured at a TOA of 80° from the spectrum measured at 15°, to eliminate spectrum arising from bulk Si after multiplying the spectrum measured at a TOA of 80° by an appropriate factor of b. Intensities of subnitride spectra in Fig. 9(c) must be affected by photoelectron diffraction because the effects of photoelectron diffraction on the I(S) at TOAs of 80° and 15° must be different.[18]

Considering the spectra arising from the $\underline{Si}-(OH)_3N$, $\underline{Si}-N_4$, and bulk Si and optimizing CSs of the subnitride spectra, the Si $2p_{3/2}$ spectrum shown in Fig. 10(a), in which the spectral intensity of Fig. 6(a) is magnified, is decomposed. The spectra having CSs of 0.25, 0.61, 0.89, and 1.23 eV can be correlated with $\underline{Si}-Si_3H$, $Si^{1+}(N)$, $\underline{Si}-Si_2NH$, and $Si^{2+}(N)$, respectively.[8] Here, $\underline{Si}-Si_3H$ denotes a Si atom bonded with one H atom and three Si atoms, $Si^{1+}(N)$ denotes a Si atom bonded with one N atom and three Si atoms, $Si^{2+}(N)$ denotes a Si atom bonded with two N atoms and two Si atoms, and $\underline{Si}-Si_2NH$, which was theoretically shown to exist at the Si_3N_4/Si interface,[19] denotes a Si atom bonded with one N atom, one H atom, and two Si atoms. The CSs of $\underline{Si}-Si_3H$, $Si^{1+}(N)$ and $Si^{2+}(N)$ roughly agree with the reported values.[7,8] Therefore, the subnitrides consist of four components. The relatively small value of 2.25–2.28 eV observed for the CS of the Si $2p$ core level in Si_3N_4 must be attributed to the decrease in its CS, in accordance with the decrease in the thickness of the Si_3N_4 film as in the case of SiO_2.[20] It should be noted that $Si^{3+}(N)$, which denotes a Si atom bonded with three N atoms and one Si atom, was not detected in Fig. 9(b). The spectrum having CS of −0.20 eV in Fig. 9(c) must be correlated with the second neighbor electronegativity effects predicted for $SiO_2/Si(100)$ interface.[21] Using the BEs of Si $2p_{3/2}$ spectra arising from the components of subnitrides formed on Si(100), the Si $2p_{3/2}$ spectra arising from subnitrides formed on Si(111) and Si(110) were decomposed as shown in Fig. 10.

Figure 11 shows the spectral intensity ratio $I(n^+)/I(N)$ as a function of TOA. Here, $I(n^+)$, whose expression is given in Appendix, denotes the intensity of the Si $2p_{3/2}$ spectrum arising from the component of subnitrides having the areal density denoted by $D(Si^{n+})$. If the subnitrides localize only at the Si_3N_4/Si interface, four solid lines shown in Fig. 11 are obtained for the calculated dependence of $I(n^+)/I(N)$ on TOA using values of four kinds of $D(Si^{n+})$, that is, $D(\underline{Si}-Si_3H)$, $D(Si^{1+})$, $D(\underline{Si}-Si_2NH)$, and $D(Si^{2+})$, which are the areal densities of $\underline{Si}-Si_3H$, $Si^{1+}(N)$, $\underline{Si}-Si_2NH$, and $Si^{2+}(N)$, respectively, listed in Table I. The dashed lines in Fig. 7 were obtained for the calculated dependence of intensity ratio I(I)/I(N) on TOA. Here, I(I) denotes the sum of spectral intensities arising from $Si^{2+}(N)$, $\underline{Si}-Si_2NH$, $Si^{1+}(N)$, and $\underline{Si}-Si_3H$. Possible bonding configurations of $\underline{Si}-Si_3H$, $Si^{1+}(N)$, $\underline{Si}-Si_2NH$, and $Si^{2+}(N)$ at the Si_3N_4/Si interface formed on Si(100) are illustrated in Fig. 12. The composition of subni-

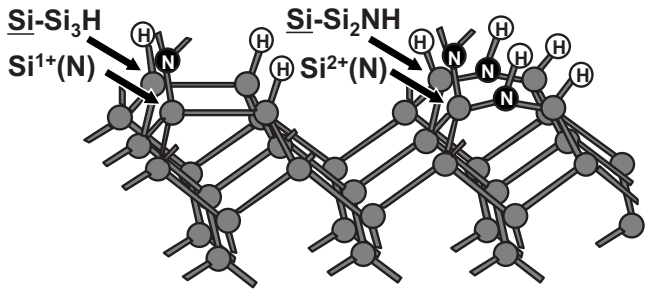

FIG. 12. Possible bonding configurations of subnitrides formed at the $Si_3N_4/Si(100)$ interface are illustrated.

trides, in other words, the interface structures depend on the crystallographic orientation of the Si substrate, mainly because the areal density of Si–H bonds, in other words, the sum of D(Si–Si_3H) and D(Si–Si_2NH), localized at Si_3N_4/Si(110) interface is 38%–53% larger than those localized at Si_3N_4/Si(100) and Si_3N_4/Si(111) interfaces. This implies that the structural imperfection terminated with H atoms at Si_3N_4/Si(110) interface is larger than those at Si_3N_4/Si(100) and Si_3N_4/Si(111) interfaces.

The experimental data in Figs. 4, 7, and 11 are not affected by the photoelectron diffraction[18] because Si–$(OH)_3N$ and Si–N_4 are in amorphous states and the subnitrides formed using NH radicals must be randomly oriented in contrast to thermally grown silicon suboxides.[22] The values of 2.28×10^{28} m^{-3} and 3.19×10^{3} kg m^{-3} were used for the atomic concentration[23] of Si in SiO_2, which is assumed to be equal to that of Si in Si–$(OH)_3N$, and the density[6] of Si_3N_4, respectively. The photoionization cross section of the Si 2*p* core level in the Si_3N_4 film and bulk Si are assumed to be the same. Because the total areal densities of subnitrides formed on Si(100), Si(111), and Si(110) are nearly equal to the areal density of Si atoms on Si(100) (6.8×10^{18} m^{-2}), Si(111) (7.85×10^{18} m^{-2}), and Si(110) (9.6×10^{18} m^{-2}), respectively, and the dependence of I(I)/I(N) on TOA calculated for all subnitrides localized at the interface are in good agreement with the experimental data as can be seen in Fig. 11, the compositional transition must be abrupt at the Si_3N_4/Si interfaces formed on Si(100), Si(111), and Si(110). Therefore, the surface morphologies of Si(100), Si(111), and Si(110) existed before the nitridation must be preserved after the nitridation. This was confirmed by the AFM observation shown in Fig. 1 that the single atomic steps on Si(100) existed before the nitridation were preserved after the nitridation. This justifies the simplified analyses of experimental data, which are expressed as the layer-by-layer growth of silicon nitride on Si(100), Si(111), and Si(110), given in the Appendix. Furthermore, the FWHMs of Si 2*p* spectra arising from bulk Si observed for Si(100), Si(111), and Si(110) are 0.409, 0.395, and 0.392 eV, respectively. Therefore, the FWHM of the Si 2*p* spectrum arising from bulk Si decreases as the areal density of Si atoms at the Si_3N_4/Si interface approach that of the Si_3N_4 film (1.17×10^{19} m^{-2}). This observation can be correlated with the dependence of stress at the Si_3N_4/Si interface on the crystallographic orientation.[24]

IV. CONCLUSION

The structure of the nitride films formed on Si(100), Si(111), and Si(110) using NH radicals was characterized by measuring soft x-ray-excited angle-resolved Si 2*p*, N 1*s* and O 1*s* photoelectron spectra. Si_3N_4 film was found to be covered with one monolayer of Si–$(OH)_3N$, which was formed by the oxidation of pure Si layer, which exists on the surface of a Si_3N_4 film after the nitridation of Si, in air just after the nitride film was removed from the nitridation chamber. Considering that the areal density of N atoms, which constitute Si–$(OH)_3N$, on Si(111) is 15% smaller than those on Si(100) and Si(110), we speculate that the areal density of Si_3N_4 on Si(111) is 15% smaller than those on Si(100) and Si(110). The compositional transition at Si_3N_4/Si interface formed on Si(100), Si(111), and Si(110) is abrupt, mainly because the Si^{3+} were not detected at these interfaces and the compositional transition layers consist of Si–Si_3H, Si^{1+}(N), Si–Si_2NH, and Si^{2+}(N). The composition of subnitrides, in other words, Si_3N_4/Si interface structures depend on the crystallographic orientation of the Si substrate, mainly because the areal density of Si–H bonds localized at the Si_3N_4/Si(110) interface is 38%–53% larger than those at the Si_3N_4/Si(100) and Si_3N_4/Si(111) interfaces. This implies the structural imperfection terminated with H atoms at the Si_3N_4/Si(110) interface is larger than those at the Si_3N_4/Si(100) and Si_3N_4/Si(111) interfaces. Because the compositional transition at Si_3N_4/Si interfaces formed on Si(100), Si(111) and Si(110) is abrupt, the surface morphologies of Si(100), Si(111), and Si(110) existed before the nitridation must be preserved after the nitridation. This was confirmed by the AFM observation that the single atomic steps on Si(100) existed before the nitridation were preserved after the nitridation.

ACKNOWLEDGMENTS

The authors gratefully acknowledge the Ministry of Economy, Trade, and Industry and The New Energy and Industrial Technology Development Organization for their financial support to the development of plasma-process equipment. This work was supported by the Japanese Ministry of Education, Culture, Sports, Science and Technology under a Grant-in-Aid for Specially Promoted Research (Project No. 18002004), a Grant-in-Aid for Scientific Research (B) (Project No. 19360014), and a Grant-in-Aid for Young Scientists (Start-up) (Project No. 18860006). The synchrotron radiation experiments were performed at SPring-8 with the approval of Japan Synchrotron Radiation Research Institute for the project of Nanotechnology Support of the Ministry of Education, Culture, Sports, Science and Technology of Japan.

APPENDIX

Although the thickness of the amorphous Si_3N_4 film probed by the photoelectron spectroscopy distributes around the average thickness, the distributions of Si_3N_4 film thicknesses are simplified in the present analyses of the photoelectron spectra. Namely, the Si_3N_4 films formed on Si(100) and Si(110) are assumed to consist of 100y% of three monolayers of Si_3N_4 and $100(1-y)$% of four monolayers of Si_3N_4 instead of two monolayers of Si_3N_4 in Fig. 13, while the Si_3N_4 film formed on Si(111) is assumed to consist of 100y% of two monolayers of Si_3N_4 as shown in Fig. 13 and $100(1-y)$% of three monolayers of Si_3N_4 instead of two monolayers of Si_3N_4 in Fig. 13. Then, the intensities of angle-resolved Si 2*p*, N 1*s*, and O 1*s* photoelectron spectra arising from the Si_3N_4 film and the Si_3N_4/Si interface can be explained quantitatively using the following equations. Here, the thickness symbols of various layers used in the following equations are defined in Fig. 13. Furthermore, after cleaning Si(111) substrate a Si atom on Si(111) surface is considered to have one broken bond terminated with H atom.[11]

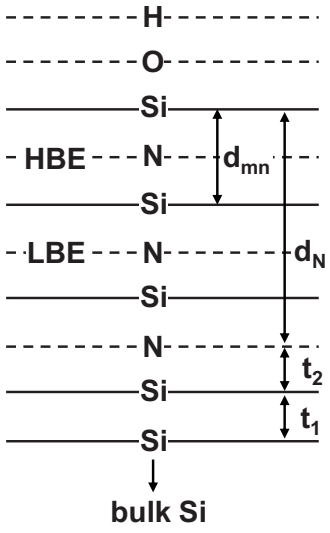

FIG. 13. Schematic diagram of $\underline{\text{Si}}-(\text{OH})_3\text{N}/\underline{\text{Si}}-\text{N}_4$/subnitrides/Si structure.

$$\begin{aligned}\text{I(S)} &\equiv \text{I(Si } 2p_{3/2}\text{, bulk Si)}\\ &= \{\text{KY(bulk Si)}\sigma\text{(Si } 2p_{3/2})\text{D}_{100}\text{(bulk Si)/R}_{100}\}\\ &\quad\times \exp\{-t_1/(\Lambda_{t1}\sin\theta)\}\exp\{-t_2/(\Lambda_{t2}\sin\theta)\}\\ &\quad\times\{f^7y + f^9(1-y)\}g \quad \text{for Si(100)},\end{aligned}$$

$$\begin{aligned}\text{I(S)} &\equiv \text{I(Si } 2p_{3/2}\text{, bulk Si)}\\ &= \text{KY(bulk Si)}\sigma\text{(Si } 2p_{3/2})\text{D}_{111}\text{(bulk Si)}\\ &\quad\times\exp\{-t_2/(\Lambda_{t2}\sin\theta)\}\\ &\quad\times[\{yf^5/\text{R}_{111}\}\exp\{-t_1'/(\Lambda_{t1}\sin\theta)\}\\ &\quad+\{(1-y)f^7/\text{R}'_{111}\}\exp\{-t_1''/(\Lambda_{t1}\sin\theta)\}]g\\ &\quad\text{for Si(111)},\end{aligned}$$

$$\begin{aligned}\text{I(S)} &\equiv \text{(Si } 2p_{3/2}\text{, bulk Si)}\\ &= \{\text{KY(bulk Si)}\sigma\text{(Si } 2p_{3/2})\text{D}_{110}\text{(bulk Si)/R}_{110}\}\\ &\quad\times\exp\{-t_1/(\Lambda_{t1}\sin\theta)\}\exp\{-t_2/(\Lambda_{t2}\sin\theta)\}\{f^7y\\ &\quad+f^9(1-y)\}g \quad \text{for Si(110)},\end{aligned}$$

$$\begin{aligned}\text{I(N)} &\equiv \text{I(Si } 2p_{3/2}\text{,Si}_3\text{N}_4)\\ &= \text{KY(Si}_3\text{N}_4)\sigma\text{(Si } 2p_{3/2})\text{D(Si}_3\text{N}_4)\\ &\quad\times\{(f^2+f^4+f^6)y + (f^2+f^4+f^6+f^8)\\ &\quad\times(1-y)\}g \quad \text{for Si(100)and Si(110)},\end{aligned}$$

$$\begin{aligned}\text{I(N)} &\equiv \text{I(Si } 2p_{3/2}\text{,Si}_3\text{N}_4)\\ &= \text{KY(Si}_3\text{N}_4)\sigma\text{(Si } 2p_{3/2})\text{D(Si}_3\text{N}_4)\\ &\quad\times\{(f^2+f^4)y + (f^2+f^4+f^6)(1-y)\}g\\ &\quad\text{for Si(111)}\end{aligned}$$

$$\begin{aligned}\text{I(O)} &\equiv \text{I(Si } 2p_{3/2}\text{,}\underline{\text{Si}}-(\text{OH})_3\text{N)}\\ &= \text{KY}(\underline{\text{Si}}-(\text{OH})_3\text{N})\sigma\text{(Si } 2p_{3/2})\text{D}(\underline{\text{Si}}-(\text{OH})_3\text{N})g\\ &\cong \text{KY(SiO}_2)\sigma\text{(Si } 2p_{3/2})\text{D}(\underline{\text{Si}}-(\text{OH})_3\text{N})g\\ &\quad\text{for Si(100), Si(111), and Si(110)},\end{aligned}$$

$$\begin{aligned}\text{I}(n^+) &\equiv \text{I(Si } 2p_{3/2}\text{, subnitride)}\\ &= \{\text{KY(subnitride)}\sigma\text{(Si } 2p_{3/2})\text{D(Si}^{n+})\}\\ &\quad\times\exp\{-t_2/(\Lambda_{t2}\sin\theta)\}\{f^7y + f^9(1-y)\}g\\ &\quad\text{for Si(100) and Si(110)},\end{aligned}$$

$$\begin{aligned}\text{I}(n^+) &\equiv \text{I(Si } 2p_{3/2}\text{, subnitride)}\\ &= \{\text{KY(subnitride)}\sigma\text{(Si } 2p_{3/2})\text{D(Si}^{n+})\}\\ &\quad\times\exp\{-t_2/(\Lambda_{t2}\sin\theta)\}\{f^5y + f^7(1-y)\}g\\ &\quad\text{for Si(111)},\end{aligned}$$

$$\begin{aligned}\text{I(N } 1s) &= \text{K}\sigma\text{(N } 1s)\{(4/3)\text{D(Si}_3\text{N}_4)\}\\ &\quad\times\{(f^3+f^5+f^7)y + (f^3+f^5+f^7+f^9)\\ &\quad\times(1-y)\}g + \text{K}\sigma\text{(N } 1s)\\ &\quad\text{for Si(100) and Si(110)},\end{aligned}$$

$$\begin{aligned}\text{I(N } 1s\text{,LBE}) &= \text{K}\sigma\text{(N } 1s)\{(4/3)\text{D(Si}_3\text{N}_4)\}\\ &\quad\times\{(f^3+f^5+f^7)y + (f^3+f^5+f^7+f^9)\\ &\quad\times(1-y)\}g\\ &\quad\text{for Si(100) and Si(110)},\end{aligned}$$

$$\begin{aligned}\text{I(N } 1s\text{,HBE}) &= \text{K}\sigma\text{(N } 1s)\text{D(N)}fg\\ &\quad\text{for Si(100) and Si(110)},\end{aligned}$$

$$\begin{aligned}\text{I(N } 1s) &= \text{K}\sigma\text{(N } 1s)\{(4/3)\text{D(Si}_3\text{N}_4)\}\\ &\quad\times\{(f^3+f^5)y + (f^3+f^5+f^7)(1-y)\}g\\ &\quad+\text{K}\sigma\text{(N } 1s)\text{D(N)}fg\\ &\quad\text{for Si(111)},\end{aligned}$$

$$\begin{aligned}\text{I(N } 1s\text{,LBE}) &= \text{K}\sigma\text{(N } 1s)\{(4/3)\text{D(Si}_3\text{N}_4)\}\\ &\quad\times\{(f^3+f^5)y + (f^3+f^5+f^7)\\ &\quad\times(1-y)\}g\\ &\quad\text{for Si(111)},\end{aligned}$$

$$\begin{aligned}\text{I(N } 1s\text{,HBE}) &= \text{K}\sigma\text{(N } 1s)\text{D(N)}fg\\ &\quad\text{for Si(111)},\end{aligned}$$

$$\begin{aligned}\text{I(O } 1s) &= \text{K}\sigma\text{(O } 1s)\{3\text{D}(\underline{\text{Si}}-(\text{OH})_3\text{N})\}\text{h}\\ &\quad\text{for Si(100), Si(111) and Si(110)},\end{aligned}$$

$$d_{\text{N}} = \{3y + 4(1-y)\}d_{\text{mn}} \quad \text{for Si(100) and Si(110)},$$

$$d_{\text{N}} = \{2y + 3(1-y)\}d_{\text{mn}} \quad \text{for Si(111)}.$$

Here, K is dependent on photon flux, but independent of θ, $\sigma(\text{Si } 2p_{3/2})$, $\sigma(\text{N } 1s)$, and $\sigma(\text{O } 1s)$ denote photoionization cross section of Si $2p_{3/2}$, N $1s$, and O $1s$ core levels, respectively, and the contribution of subnitrides to N $1s$ spectra is

neglected. The ratio $\sigma(\mathrm{O}\ 1s)/\sigma(\mathrm{N}\ 1s)$ takes a value of 1.24, which is interpolated from the dependence of photoionization cross section on the photon energy.[25] The attenuation factor f, which is expressed by $\exp\{-(d_{\mathrm{mn}}/2)/(\Lambda_{\mathrm{bn}}\sin\theta)\}$ using the thickness of Si_3N_4 monolayer denoted by d_{dm}, is used to describe the decrease in the spectral intensities by inelastic scattering in a half-monolayer of Si_3N_4. The attenuation factors g and h are used to describe the decrease in the Si $2p_{3/2}$ and N 1*s* spectral intensities by inelastic scattering of photoelectrons arising from Si $2p_{3/2}$ and N 1*s* core levels with O-H in Fig. 5 and the decrease in the O 1*s* spectral intensities by inelastic scattering of photoelectrons arising from O 1*s* core levels with H atoms in Fig. 5, respectively. D_{hkl}(bulk Si) and R_{hkl} were defined by Himpsel *et al.*[17]

Between layers one has the following attenuation factor of $q_{\mathrm{hkl}}=\exp\{-d_{\mathrm{hkl}}/(\Lambda_{\mathrm{bs}}\sin\theta)\}$, with $d_{100}=0.136$ nm, $d_{111}=0.0784$ nm, and $d_{110}=0.192$ nm. For Si(100) and Si(110) one has the following expression:[17] $\mathrm{R}_{\mathrm{hkl}}=1-q_{\mathrm{hkl}}$. For Si(111), one has the following expressions:[17] $\mathrm{R}_{111}=(1-q_{111}^4)/(1+q_{111})$ and $\mathrm{R}'_{111}=(1-q_{111}^4)/(1+q_{111}^3)$.

The following values were used: D_{100}(bulk Si)$=6.8\times10^{18}$ m^{-2}, D_{111}(bulk Si)$=7.8\times10^{18}$ m^{-2}, D_{110}(bulk Si)$=9.6\times10^{18}$ m^{-2}, c_{bn} (Si atomic density in the Si_3N_4)$=4.11\times10^{28}$ m^{-3}, c_{bo} (Si atomic density in the SiO_2)$=2.28\times10^{28}\mathrm{m}^{-3}$, $d_{\mathrm{mn}}=c_{\mathrm{bn}}^{-1/3}=0.29$ nm, Λ_{bn} (electron escape depth in the Si_3N_4)$=2.41$ nm,[26] Λ_{bs} (electron escape depth in the bulk Si)$=1.59$ nm, and Λ_{bo} (electron escape depth in the SiO_2)$=2.86$ nm,[26] respectively. Furthermore, we assume t_2 (thickness of second transition layer)$\cong d_{\mathrm{mn}}/2=0.145$ nm, t_1 (thickness of first transition layer)$\cong d_{100}$ for Si(100), $t_1\cong d_{110}$ for Si(110), $t'_1\cong d_{111}$ and $t''_1\cong 3d_{111}$ for Si(111), Λ_{t2} (electron escape depth in the second transition layer)$\cong(\Lambda_{\mathrm{bn}}+\Lambda_{\mathrm{bs}})/2=2$ nm, and Λ_{t1} (electron escape depth in the first transition layer)$\cong\Lambda_{\mathrm{bs}}$.

$\mathrm{Y}(Si_3N_4)$, Y(bulk Si), and $\mathrm{Y}(SiO_2)$ denote the photoelectron yields (the percentage of Si 2*p* photoelectrons which escape without undergoing inelastic scattering) in the Si_3N_4, bulk Si, and SiO_2, respectively.[27] The yield is obtained by dividing the area of the Si 2*p* peak by the sum of the areas of the Si 2*p* peak and all the measurable plasmon loss peaks.[27] We found $\mathrm{Y}(Si_3N_4)=0.841$, Y(bulk Si)$=0.617$, and $\mathrm{Y}(SiO_2)=0.887$.

[1] G. D. Wilk, R. M. Wallace, and J. M. Anthony, J. Appl. Phys. **89**, 5243 (2001).
[2] K. Sekine, Y. Saito, M. Hirayama, and T. Ohmi, IEEE Trans. Electron Devices **47**, 1370 (2000).
[3] H. Shimada, I. Ohshima, S. Nakao, M. Nakagawa, K. Kanemoto, M. Hirayama, S. Sugawa, and T. Ohmi, Symp. on VLSI Technology, p. 67 (2001).
[4] T. Ito, S. Hijiya, T. Nozaki, H. Arakawa, M. Shinoda, and Y. Fukukawa, J. Electrochem. Soc. **125**, 448 (1978).
[5] Y. Hayafuji and K. Kajiwara, J. Electrochem. Soc. **129**, 2102 (1982).
[6] C. Maillot, H. Roulet, G. Dufour, F. Rochet, and S. Rigo, Appl. Surf. Sci. **26**, 326 (1986).
[7] C. H. F. Peden, J. W. Rogers, Jr., N. D. Shinn, K. B. Kidd, and K. L. Tsang, Phys. Rev. B **47**, 15622 (1993).
[8] M. Higuchi, S. Sugawa, E. Ikenaga, J. Ushio, H. Nohira, T. Maruizumi, A. Teramoto, T. Ohmi, and T. Hattori, Appl. Phys. Lett. **90**, 123114 (2007).
[9] S. Tanuma, S. C. J. Powell, and D. R. Penn, Surf. Interface Anal. **20**, 77 (1993).
[10] Y. Morita and H. Tokumoto, Appl. Surf. Sci. **100-101**, 440 (1996).
[11] T. Ohmi, J. Electrochem. Soc. **143**, 2957 (1996).
[12] M. Hirayama and T. Ohmi, Proceedings of the 1997 Joint International Meeting, Paris, August–September 1997 (unpublished), Vols. 97, pp. 1802–1803.
[13] S. Carniato, J.-J. Gallet, F. Rochet, G. Dufour, F. Boumel, S. Rangan, A. Verdini, and L. Floreano, Phys. Rev. B **76**, 085321 (2007).
[14] J. Ushio, T. Maruizumi, and K. Kushida-Abdelghafar, Appl. Phys. Lett. **81**, 1818 (2002).
[15] H. Nohira, N. Tamura, J. Ushio, and T. Hattori, Proc.-Electrochem. Soc. **2005**, 19 (2005).
[16] K. Ohishi and T. Hattori, Jpn. J. Appl. Phys., Part 2 **33**, L675 (1994).
[17] F. J. Himpsel, F. R. McFeely, A. Talev-Ibrashimi, J. A. Yarmoff, and G. Hollinger, Phys. Rev. B **38**, 6084 (1988).
[18] K. Takahashi, K. Hirose, H. Nohira, and T. Hattori, Appl. Phys. Lett. **83**, 3422 (2003).
[19] G.-M. Rignanese and A. Pasquarello, Phys. Rev. B **63**, 075307 (2001).
[20] Th. Eickhoff, V. Medicherla, and W. Drube, J. Electron Spectrosc. Relat. Phenom. **137-140**, 85 (2004).
[21] O. V. Yazyev and A. Pasquarello, Phys. Rev. Lett. **96**, 157601 (2006).
[22] S. Dreiner, M. Schürmann, C. Westphal, and H. Zacharias, Phys. Rev. Lett. **86**, 4068 (2001); S. Dreiner, M. Schürmann, and C. Westphal, *ibid.* **93**, 126101 (2004).
[23] M. F. Hochella, Jr. and A. H. Carim, Surf. Sci. **197**, L260 (1988).
[24] A. Ogura, T. Yoshida, D. Kosemura, Y. Kakemura, T. Aratani, M. Higuchi, S. Sugawa, A. Teramoto, T. Ohmi, and T. Hattori, Appl. Surf. Sci. **254**, 6229 (2008).
[25] M. B. Trzhaskovskaya, V. I. Nefedov, and V. G. Yarzhemsky, At. Data Nucl. Data Tables **77**, 97 (2001).
[26] T. Hattori, H. Nohira, S. Shinagawa, M. Hori, M. Kase, and T. Maruizumi, Microelectron. Reliab. **47**, 20 (2007).
[27] Z. H. Lu, J. P. McCaffrey, B. Brar, G. D. Wilk, R. M. Wallance, and L. C. Feldman, Appl. Phys. Lett. **71**, 2764 (1997).